Peer-reviewed version available at Metals 2018, 8, 512; doi:10.3390/met8070512

Article

Characteristics of Welding and Arc Pressure in the Plasma–TIG Hybrid Welding Process

Bo Wang [1,2], Xunming Zhu [3], Hongchang Zhang [4,*], Hongtao Zhang [1,2,*] and Jicai Feng [1]

[1] State Key Laboratory of Advanced Welding and Joining, Harbin Institute of Technology, Harbin 150001, China; wangvbo@hit.edu.cn; zhanght@hitwh.edu.cn; fengjc@hit.edu.cn

[2] Shandong Institute of Shipbuilding Technology, Weihai 264209, China; wangvbo@hit.edu.cn; zhanght@hitwh.edu.cn

[3] Weihai Wanfeng Magnesium Sciecne and Technology Development Co.Ltd, Weihai 264209, China; xunming.zhu@wfjt.com

[4] Harbin University of Science and Technology Rongcheng Campus, Rongcheng, 264300, China; 794230001@qq.com

* Correspondence: zhanght@hitwh.edu.cn; Tel.: +86-187-6910-2227; 794230001@qq.com; Tel: +86-17863082611

Abstract: In this article, a novel hybrid welding process called plasma-TIG coupled arc welding was proposed to improve the efficiency and quality of welding by utilizing the full advantage of plasma and TIG welding processes. The two arcs of plasma and TIG were pulled into each other into one coupled arc under the effect of Lorentz force and plasma flow force during welding experiments. The arc behavior of coupled arc was studied by means of it's arc profile, arc pressure and arc force conditions. The coupled arc pressure distribution measurements were performed. The effects of welding conditions on coupled arc pressure were evaluated and the maximum coupled arc pressure was improved compared with single-plasma arc and single-TIG arc. It was found that the maximum arc pressure was mainly determined by plasma arc current and plasma gas flow. According to the results, the proposed coupled arc welding process have both advantages of plasma arc and TIG method, and it has a broad application prospect.

Keywords: plasma-TIG; coupled arc; arc profile; pressure distribution

1. Introduction

Given the continuous development of processing and manufacturing technologies, traditional arc welding techniques, such as plasma arc welding (PAW)[1] and tungsten inert gas (TIG)[2,3] welding process, have been improved to meet the requirements of enterprises for high-quality and low-consumption welding technology[4]. In recent years, hybrid welding methods are proposed to overcome these disadvantages and deficiencies. Hybrid welding methods have also been successfully applied in shipbuilding and spacecraft. Certain hybrid welding processes, including plasma–MIG[5,6], plasma–TIG[7,8], laser–GMAW[9], laser–TIG[10] and TIG–MIG[11], have been successfully used in the manufacturing industry. In comparison with ordinary single-arc welding, hybrid welding technology can significantly improve welding efficiency and joint quality because it is simultaneously provided with multiple heat sources that complement one another[5].

PAW produces arc plasma with high energy density and high arc pressure under the thermal pinch effect of the water-cooled copper nozzle; thus, PAW has strong fusion and penetration

abilities[12,13]. However, identifying the appropriate parameters in PAW welding process is difficult and the process is prone to undercutting[14]. The gas tungsten arc welding with DCEN (Direct Current Electrode Negative Epolarity) is an high efficiency welding process[15,16], and has a good surface forming ability and remarkably stable welding process, but it's penetration capacity is poor. Therefore, researchers also proposed several hybrid welding processes that utilize the PAW and TIG arcs, which mainly include the double-sided arc welding (DSAW) and PAW–TIG welding processes[8]. The DSAW process can increase penetration and significantly improve welding productivity[17], in this process, a TIG torch is placed on the opposite side of welds to guide the PAW arc into the keyhole, thereby permitting the current to flow from the PAW torch through the welds to the TIG torch directly instead of the conventional welding current loop[7,18]. However, the welding accessibility of DSAW is poor compared with PAW welding process. The PAW–TIG welding method is realized by the PAW and the subsequent TIG on the movable slide rail, no correlation exists between the plasma and TIG arcs. This process can also enhance the welding productivity. However, the heat-affected zone is large and the grain is coarse because the weld is reheated by the TIG arc. The plasma–TIG coupled arc welding (PTCAW) process is a novel hybrid welding method for overcoming the above deficiencies in order to achieve efficient welding process and high-quality welds.

In this study, the PTCAW process was initially constructed and the coupled arc profile was then analyzed by a charge-coupled device (CCD) camera. The effects of welding conditions on the coupled arc pressure distribution was also studied to reveal the characteristics of the coupled arc welding process The results provided the basis to recognize the PTCAW process and expanded the application range of PAW and TIG welding processes.

2. Materials and Methods

The schematic diagram of our experimental set-up is shown in Fig. 1. The PAW and TIG torches were fixed on one fixture to realize the interaction between the two processes (i.e., PTCAW process). An experimental system was established according to the above designed principle. In the present system, the TIG arc was established by using a direct current–constant current (DC–CC) power supply (REHM InverTIG.Pro digital 240 AC/DC) under the direct current electrode negative(DCEN) condition. The PAW arcs were established by using an alternating current–direct current AC/DC (LORCH V50 AC/DV) and DC–CC (LORCH Handy TIG 180 DC) power supplies. The Xiris XVC-1000 weld camera (55 frames/s) was applied to observe and capture the arc profile and behavior under the different welding condition in real time[19]. The anode constricting nozzle of PAW made of red cooper with excellent thermal conductivity is cooled by forced recirculation cooling water to prevent the nozzle from being burned.

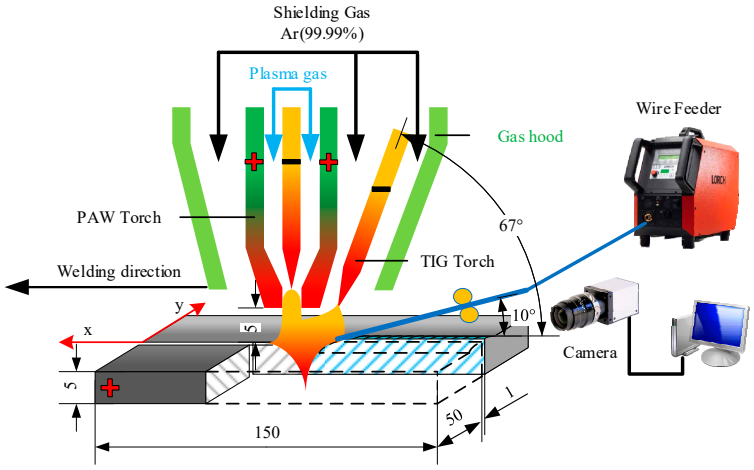

Fig. 1. Proposed PTCAW process system.

Preprints (www.preprints.org) | NOT PEER-REVIEWED | Posted: 30 May 2018 doi:10.20944/preprints201805.0446.v1

Peer-reviewed version available at Metals 2018, 8, 512; doi:10.3390/met8070512

Differential pressure sensor (DPS: HSTL-FY01) was used to detect the arc pressure and pressure distribution[20-22]. A 0.8-mm-diameter hole was drilled on a copperplate, which was fixed on another water-cooled copperplate[23]. The details of the measurement system are shown in Fig. 2.

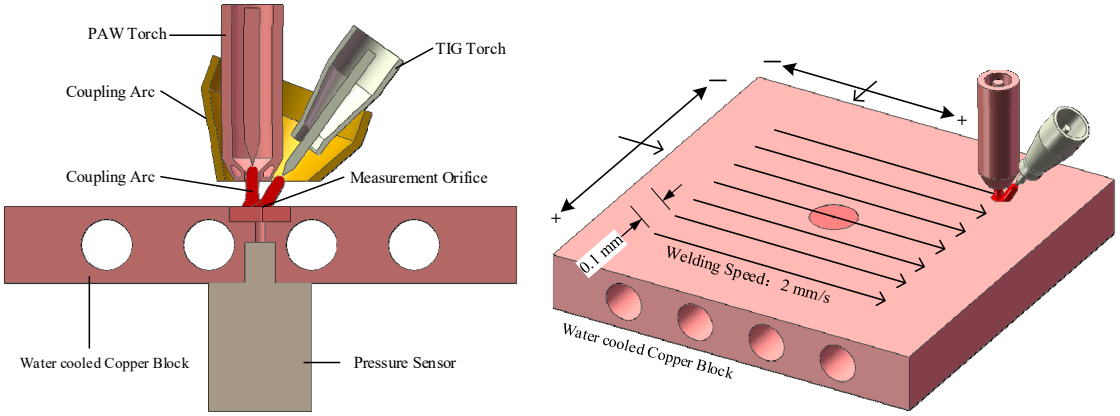

Fig. 2. Measurement system of the arc pressure.

In all experiments, the PAW torch nozzle has a 3-mm orifice diameter, 3.2-mm tungsten diameter, and 3-mm tungsten setback. Pure argon (99.99%) was used as the plasma gas and shielding gas. The platform diameter of the TIG terminal electrode is 1.25 mm, and the shielding gas flow rate is 15 L/min. The electrode spacing is 7 mm, that is the distance from the plasma nozzle axis to the electrode tip of TIG. The nozzle height is the distance from the end of PAW nozzle to the workpiece surface. The detailed parameters for the designed experiments are shown in Table 2.

Table 2 Welding parameters for designed experiments.

Group	Plasma arc current (A)	TIG arc current (A)	Nozzle height (mm)	Plasma gas flow (L/min)
#1	60, 80, 100, 120	100	5	4
#2	60	60, 90, 120, 150	5	4
#3	120	140, 160, 180, 200	5	4
#4	60	100	3, 4, 5, 6	4
#5	60	100	5	3, 4, 5, 6

3. Results and discussion

3. Results and Discussions

3.1. TPTCAW coupled arc profile

A notable characteristic of the plasma-TIG welding method is the physical coupling effect between the two arcs, which results in penetration increased and splash rate descended. The detailed images of the plasma, TIG, and coupled arcs were acquired as shown in Figs.4. The RGB images in the figure were transformed from gray images through pseudo-color processing in order to acquire more detailed information of the arc profile. The base plate is made of red copper with forced recirculation cooling water and the welding experiment was carried out under the following conditions: a plasma welding current of 60A while TIG current of 100A, nozzle height of 5 mm and plasma gas flow of 15 L/min.

Figure 3 illustrates typical arc profile under different welding methods. Welding arcs is steady and plasma arc seems to be trumpet-shaped while TIG arc is similar to broom-shaped during single arc welding because of the tungsten axis and the base plate have a 67 degrees angle, as shown in

Fig.3a & b. When the TIG arc is applied to plasma welding arc, it is observed that a novel coupled arc is produced between the two arcs and the arc profile has a significant change from the previous. TIG arc can be deflected to plasma arc from the view of perpendicular to welding direction, and part of TIG arc is pushed to the side of plasma arc root, as shown in Fig.3c. At the same time, the coupled arc profile seems to be bell-shaped similar to the conventional TIG arc from the view of parallel to the welding direction, as shown in Fig.3d.The reason for this behavior can be explained as follows.

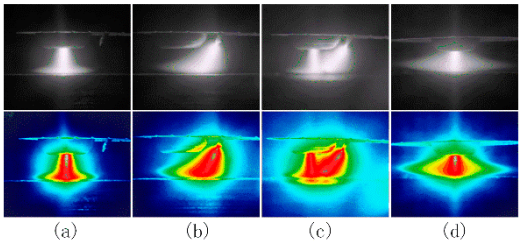

Fig. 3. Arc profile under different welding methods. **a** single plasma arc. b single TIG arc. c coupled arc perpendicular to the welding direction. d coupled arc parallel to the welding direction.

Previous studies have suggested the forces play a major role in determining the arc profile[24]. Therefore, it is necessary to analyze coupled arc force condition in order to explore the interaction mechanism on coupled arc profile. It should be noted that the electromagnetic axial pressure and plasma gas flow axial pressure are recognized as the key factor of PAW arc pressure[25]. The plasma arc radius of arc column is r_1, and the arc radius constricts to the minimum at the place of the arc root, here is r_2. The electromagnetic axial pressure on the arc axis can be expressed as the following Eq. (1),

$$p_e = \frac{\mu_0 I^2}{4\pi^2}\left(\frac{1}{r_2^2}-\frac{1}{r_1^2}\right) \tag{1}$$

Where μ_0 = permeability of free space, I = plasma arc welding current. The plasma gas flow axis pressure towards to the molten pool surface can be expressed as the following Eq. (2).

$$p_g = \frac{1}{2}\rho\mu_1^2 \tag{2}$$

Where ρ = plasma gas density, μ_1 = axial component of the plasma velocity. The plasma arc total pressure P_t on the arc axis can be expressed as the following Eq. (3).

$$p_t = p_e + p_g = \frac{\mu_0 I^2}{4\pi^2}\left(\frac{1}{r_2^2}-\frac{1}{r_1^2}\right)+\frac{1}{2}\rho\mu_1^2 \tag{3}$$

Where P_e = electromagnetic axial pressure, and it is the function of I^2. P_g = plasma gas flow axial pressure, and it is the function of ρ and μ_1, simultaneously μ1 is the function of temperature. Hence, the resultant force on the arc axis from electrode tip to the surface of base plate can be expressed as the following Eq. (4).

$$F_r = p_t \cdot S = \frac{\mu_0 I^2}{4\pi}\left(\frac{r_1^2}{r_2^2}-1\right)+\frac{1}{2}\pi\rho\mu_1^2 r_1^2 \tag{4}$$

Where F_r = the plasma arc axis resultant force, S = the arc sectional area at the place of base plate on the arc radial and $S = \pi r_1^2$. Compared with the arc force condition during the single TIG

Preprints (www.preprints.org) | NOT PEER-REVIEWED | Posted: 30 May 2018 doi:10.20944/preprints201805.0446.v1

Peer-reviewed version available at Metals 2018, 8, 512; doi:10.3390/met8070512

welding, the Lorentz force (F_L) has a significant effect on TIG arc owing to plasma arc generates additional magnetic field acts on the welding arc, and F_L can be expressed as the following Eq. (5).

$$F_L = BIL \tag{5}$$

Where B = magnetic induction of magnetic field generated by plasma arc, L = displacement of particle per unit. The schematic of the arc force condition as shown in Fig. 4. Considering the difference of arc force conditions on either side of TIG arc axis, it is necessary to specify four particles (location A, B, C and D) as the research objects. On the side of the TIG arc, the plasma flow force is considered as the main arc force of TIG welding arc, the plasma flow force can be expressed as the following Eq. (6).

$$F_P = KI^2 \log(\frac{R_b}{R_a}) \tag{6}$$

Where F_t = the plasma flow force of TIG arc at location B, C and D. K is a constant and K = $\mu/4\pi$, μ = medium magnetic conductivity, R_a and R_b are the radius of arc root surface and undersurface respectively as shown in Fig. 5c.

As seen in Fig. 4 and Fig. 3c, the direction of plasma flow force (F_{p2}) on the arc axis can be deflected to plasma arc at the location B, as shown in Fig. 5a. Furthermore, the plasma flow force acts as the major driver force of the arc shift and has important influence on the weld surface forming. According to right-hand grip rule at the location A, the direction of magnetic field generated by plasma arc current is perpendicular to the paper inward on the side of TIG arc. Hence the particles on the right side of plasma arc axis move towards plasma arc along the base plate under Lorentz force (F_{L1} and F_{L2}), the motion of TIG arc can be seen in Fig. 5a & c. At the same time, the plasma arc is also deflected slightly towards the location B owing to the Lorentz force (F_{L3}), as shown in Fig. 5 a & b. In addition, part of particles of TIG arc have a potential of coupling with that of plasma arc root, which result in transformation of TIG arc trajectory. These results indicate that the above analysis of the coupled arc force conditions is consistent with the acquired experimental results in Fig. 3. It can be concluded that the TIG arc is deflected under the combination effect of plasma flow force and Lorentz force generated by the magnetic field of plasma arc column.

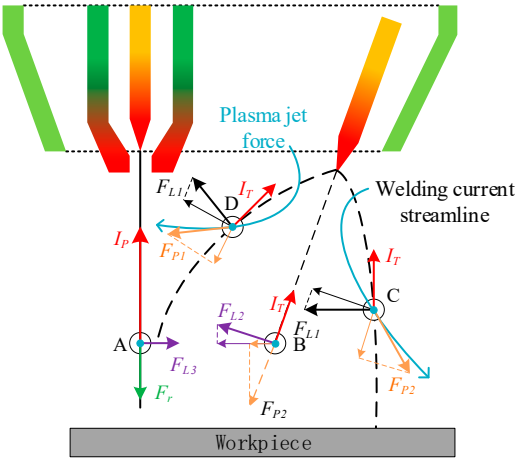

Fig. 4. Schematic of the forces acting on the coupled arcs

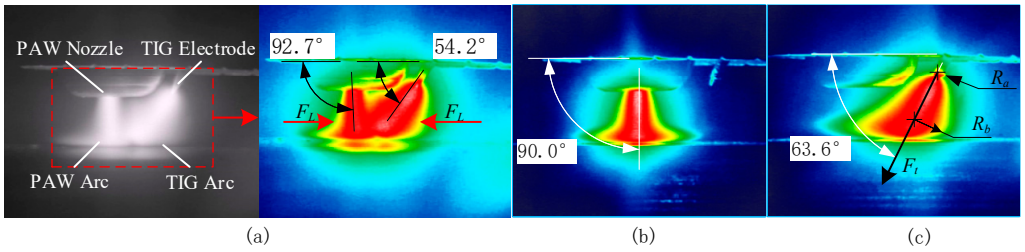

Fig. 5. Schematic of the behavior on the plasma arc Images of arc profile of different welding method. a coupled arc welding. b plasma arc welding. c TIG arc.

Therefore, according to the aforementioned analysis, another interesting finding has caught our attention. It is important to highlight that the coupling of two arcs and plasma flow force of arc are proportional to the welding current, this phenomenon is in good consistent with Eq. (4) and Eq. (6). As can be seen from Fig. 6, the coupled arc is generated only when the plasma arc current is bigger than 60A, at the same time, the arc climbing height on plasma arc column increases with welding current (I_P) when the TIG welding current (I_T) is constant at 100 amperes. However, as plasma arc current is constant at 60amperes, the plasma flow force (F_{P2}) has a marked effect on welding arc profile acting on the base plate, the heat transfer area of coupled arc acting on the workpiece is apparently increased with increase of welding current (I_T), as shown in Fig. 7.

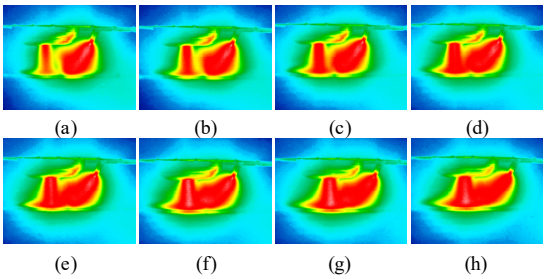

Fig. 6. Acquired images of coupled arc profile with different TIG welding current. **a** 30A. **b** 40 A. **c** 50A. **d** 60 A. **e** 70 A. **f** 80 A. **g** 90 A. **h** 100A.

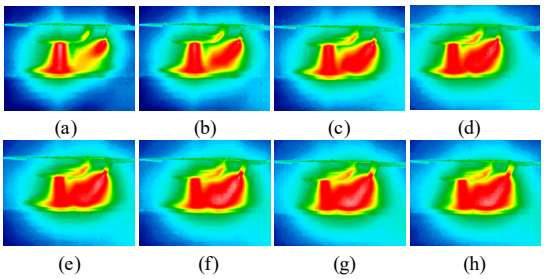

Fig. 7. Acquired images of coupled arc profile with different plasma welding current. **a** 40A. **b** 60 A. **c** 80A. **d** 100 A. **e** 120 A. **f** 140 A. **g** 160 A. **h** 180A.

3.2 Arc pressure distribution of the coupled arc

The two-dimensional pressure distribution and pressure variation along with the welding direction for each welding arc are shown in Fig. 8. The surface charts for individual stagnation pressure of three welding method are drawn using Matlab® software in order to illustrate the difference in magnitude between the values of arc pressure. According to the following experimental results, there is another interesting finding that catches our attention. It is worthwhile mentioning that the coupled arc pressure is mainly determined by plasma arc and proportion to the welding current, and the welding conditions are listed in Table 3. The contour cloud image of the

Preprints (www.preprints.org) | NOT PEER-REVIEWED | Posted: 30 May 2018 doi:10.20944/preprints201805.0446.v1

Peer-reviewed version available at Metals 2018, 8, 512; doi:10.3390/met8070512

coupled arc pressure distribution is shown in Fig. 8e, notably, it is similar to a gourd shape and the maximum arc pressure appears between the two arcs near the side of plasma arc compared with conventional plasma arc welding method. It can be seen that the maximum value of the coupled arc is approximately 650 Pa and the maximum arc pressure decreased gradually with the increasing electrode spacing, as shown in Fig. 9f. This result is significantly higher than that of plasma arc and TIG arc under the same conditions, as shown in Fig. 9b & d. Therefore, it is indicated that the total arc pressure of coupled arc depends on combination effect of these arcs, and it is consistent with the above analysis of coupled arc profile.

Table 3 Experimental conditions for arc pressure measurement

I_P (A)	I_T (A)	D_{PT} (mm)	L (mm)	D (mm)	Q_p (L/min)	Q_s (L/min)
60	100	7	5	1.25	4	15

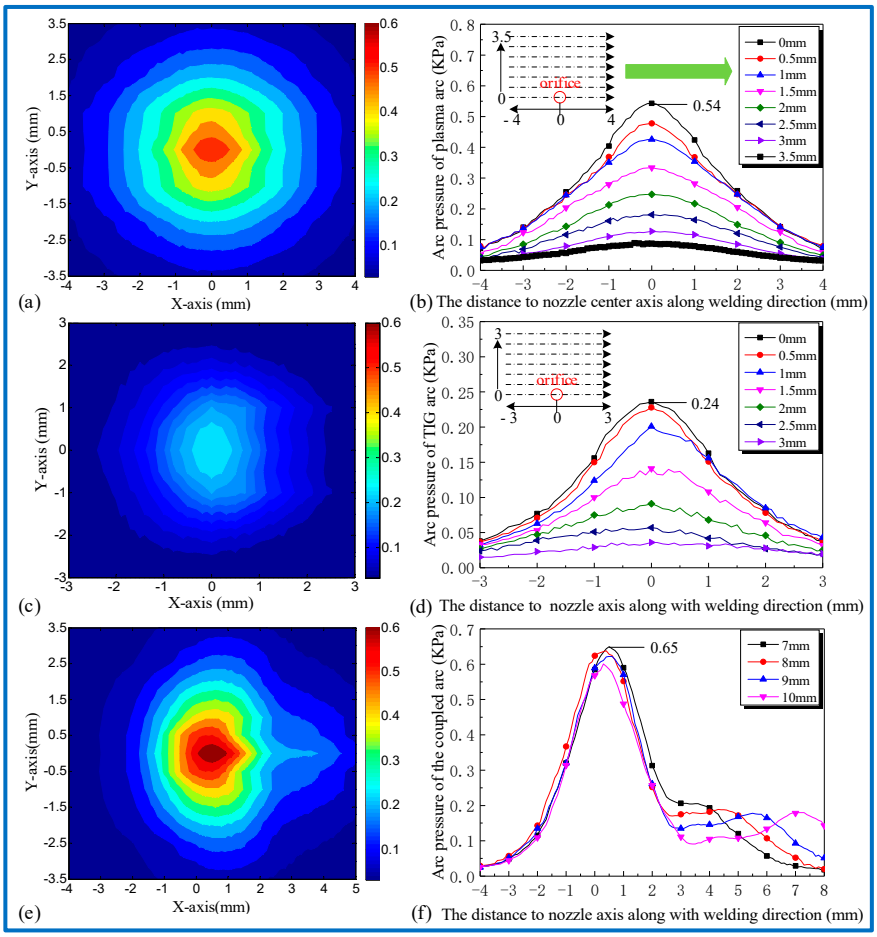

Fig. 8 Stagnation pressure distribution of welding arc with the different method. **a** top view of two-dimensional distribution of the plasma arc. **b** the plasma arc pressure along with welding direction with different distance to measurement orifice axis. **c** top view of two-dimensional distribution of the TIG arc. **d** the TIG arc pressure along with welding direction with different distance to measurement orifice axis. **e** top view of two-dimensional distribution of the coupled arc. **f** the coupled arc pressure along with welding direction with different electrode spacing.

Preprints (www.preprints.org) | NOT PEER-REVIEWED | Posted: 30 May 2018 doi:10.20944/preprints201805.0446.v1

Peer-reviewed version available at Metals 2018, 8, 512; doi:10.3390/met8070512

3.3 The influence factor of coupled arc pressure

Group #1 is the single-factor experiment to examine the effects of plasma current on the coupled arc pressure distribution. The plasma arc as an important part of the coupled arc[26], the variation in the current value has a significant influence on plasma flow force and mainly determines the maximum arc pressure of the coupled arc. The histogram of the coupled arc pressure is acquired by means of extracting the maximum value of distributed line type, as shown in Fig.9b.As can be seen from part a and b of Fig. 9, the maximum arc pressure increases gradually with the rise in plasma current and reaches 1600 Pa as plasma current is 120 amperes. In addition, according to the changes of arc pressure curves at point a, it can be illustrated that the TIG arc pressure peak is overlapped with that of plasma gradually with increase of plasma current, that is due to increase in Lorentz force during the process. This result suggest that the coupling effect is strengthened between the two arcs with the increase of plasma current.

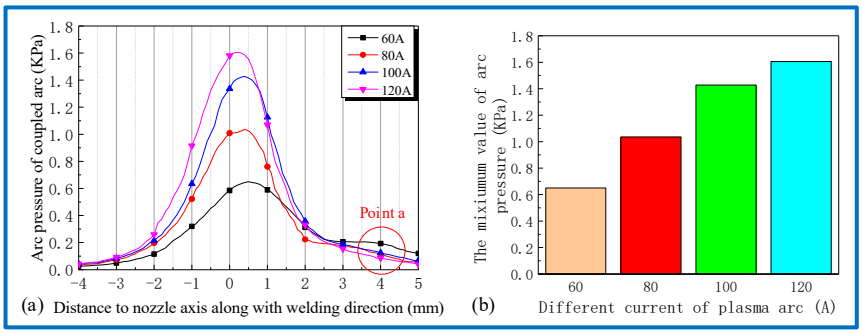

Fig. 9. Coupled arc pressure with different plasma current. **a** coupled arc pressure along with welding direction. **b** Max value of coupled arc pressure.

Groups #2 and #3 are the single-factor experiments to examine the effect of TIG current on the coupled arc pressure distribution. As previously mentioned, the change in TIG arc would has different effects on the coupled arc pressure. It is necessary to analysis the arc pressure in two situation, when the plasma arc current is 60 amperes, as shown in Fig. 10a, as the TIG current increases, the maximum arc pressure of the coupled arc gets deviated to the side of TIG arc within a small scale. This condition was mainly attributed to plasma flow force increases with welding current, it results in an good TIG arc stiffness. On the contrary, when the plasma current increases to 120 amperes, as shown in Fig. 10b, the maximum arc pressure of the coupled arc gets deviated to TIG arc by a large margin, the results indicate that the Lorentz force acting on plasma arc increases enough to deflect the plasma as the TIG current increases. This is consistent with the observation from the coupled arc profile.

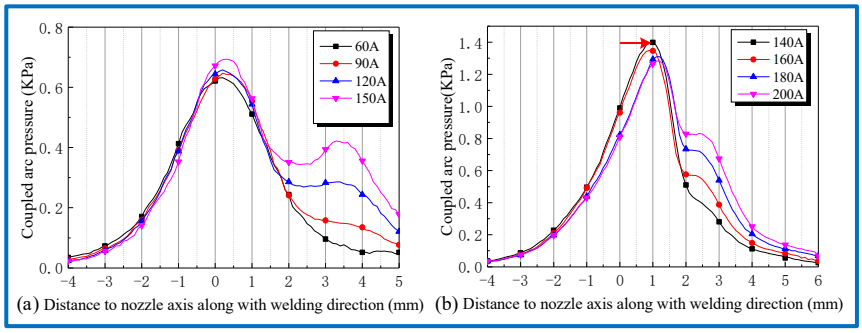

Fig. 10. Coupled arc pressure along with welding direction with different current

Group #4 is the single-factor experiment to examine the effect of the coupled arc length on the coupled arc pressure distribution. The histogram of coupled arc along with the welding direction is

acquired by means of extracting the maximum value of distributed line type, as shown in Fig. 11b. The maximum arc pressure initially decreased rapidly with the increase of nozzle height and then plateaued; meanwhile, another interesting finding is that the coupled arc no longer decreases as the nozzle height exceeds 5 mm. The results suggest that the horizontal component of the Lorentz force and plasma flow force cancels each other and reach equilibrium state along with welding direction, as shown in Eq. (5).

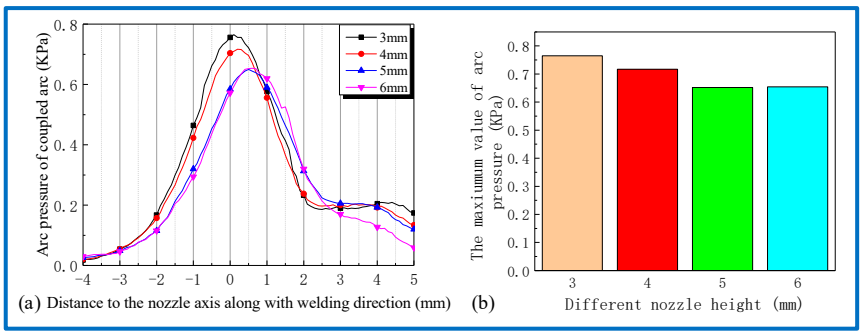

Fig. 11. Coupled arc pressure with different nozzle height. **a** coupled arc pressure along with welding direction. **b** Max value of coupled arc pressure.

Group #5 is the single-factor experiment to examine the effect of plasma gas flow rates on the coupled arc pressure distribution. Plasma gas flow rates (QP) has a significant effect on plasma movement during welding process[27]. As shown in Fig. 12, the maximum arc pressure of the coupled arc evidently increased with the increase of the plasma gas flow, it can be inferred that due to increased plasma gas flow lead to the increase in axial component of plasma velocity and plasma gas density, as shown in Eq. (2).

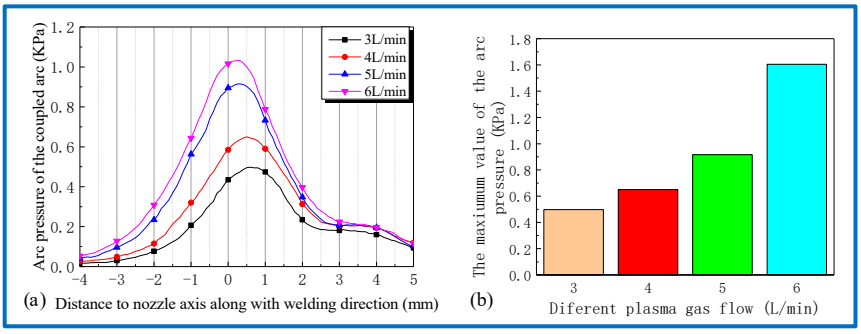

Fig. 12. Coupled arc pressure with different plasma gas flow. **a** coupled arc pressure along with welding direction. **b** Max value of coupled arc pressure.

4. Conclusions

From the current study, a novel hybrid welding method has been proposed, and the coupled arc behavior has been explored. The coupled arc profile and coupled arc pressure have been considered as ascertaining the mechanics circumstance of coupled arc behavior. The following conclusions could be obtained:

1. Under the function of Lorentz force and plasma flow force, TIG arc is deflected and couples with plasma arc, a coupled arc is generated and involves at once the arc characteristics of plasma and TIG.

2. The coupled arc profile is mainly determined by the combination effect of plasma flow force and Lorentz force generated by the magnetic field of plasma arc column, which is affected by the welding current from plasma and TIG.

3. The coupled arc pressure distribution in two-dimensional surface is similar to gourd shape, the maximum arc pressure appears between plasma arc and TIG arc and it is mainly determined by the plasma current. The welding conditions that affect the coupled arc distribution and the maximum pressure could be ranked according to their effects on the experimental results, namely, plasma current, plasma gas flow, TIG current and electrode spacing.

Author Contributions: Hongtao Zhang and Bo Wang conceived and designed the experiment; Hongchang Zhang perform the experiments; Bo Wang analysed the data and wrote the article; Xunming zhu and Jicai Feng contributed to the data analysis and discussion.

Acknowledgments: The research was sponsored by Shandong Provincial Natural Science Foundation (ZR201709200029), Shandong Key research and development plan (2017GGX30132), Shandong Key research and development plan (GG201709250277), Natural Scientific Reasearch Foundation in Harbin Institute of Technology (HIT.NSRIF.201707) and Young Taishan Scholars Program of Shandong Province (tsqn20161062) .

Conflicts of Interest: The authors declare no conflict of interest.

References

1. Liu, Z.M.; Cui, S.; Luo, Z.; Zhang, C.; Wang, Z.; Zhang, Y. Plasma arc welding: Process variants and its recent developments of sensing, controlling and modeling. *Journal of Manufacturing Processes* **2016**, *23*, 315-327.
2. Wu, C.S.; Ushio, M.; Tanaka, M. Analysis of the tig welding arc behavior. *Computational Materials Science* **1997**, *7*, 308-314.
3. Tarng, Y.S.; Tsai, H.L.; Yeh, S.S. Modeling, optimization and classification of weld quality in tungsten inert gas welding. *International Journal of Machine Tools and Manufacture* **1999**, *39*, 1427-1438.
4. Huang, J.; He, X.; Guo, Y.; Zhang, Z.; Shi, Y.; Fan, D. Joining of aluminum alloys to galvanized mild steel by the pulsed de-gmaw with the alternation of droplet transfer. *Journal of Manufacturing Processes* **2017**, *25*, 16-25.
5. Asai, M.S.; Ogawa, M.T.; Ishizaki, M.Y.; Minemura, M.T.; Minami, M.H.; Iyazaki, M.S.M. Application of plasma mig hybrid welding to dissimilar joints between copper and steel. *Welding in the World Le Soudage Dans Le Monde* **2013**, *56*, 37-42.
6. Yurtisik, K.; Tirkes, S.; Dykhno, I.; Gur, C.H.; Gurbuz, R. Characterization of duplex stainless steel weld metals obtained by hybrid plasma-gas metal arc welding. *Soldagem & Inspecao* **2013**, *18*, 207-216.
7. Zhang, Y.M.; Zhang, S.B. Double-sided arc welding increases weld joint penetration. *Welding Journal* **2000**, *77*, 57-61.
8. Taban, E. Joining of duplex stainless steel by plasma arc, tig, and plasma arc+tig welding processes. *Materials and Manufacturing Processes* **2008**, *23*, 871-878.
9. Acherjee, B. Hybrid laser arc welding: State-of-art review. *Optics & Laser Technology* **2018**, *99*, 60-71.

10. Liming, L.; Jifeng, W.; Gang, S. Hybrid laser–tig welding, laser beam welding and gas tungsten arc welding of az31b magnesium alloy. *Materials Science and Engineering: A* **2004**, *381*, 129-133.
11. Chen, J.; Wu, C.S.; Chen, M.A. Improvement of welding heat source models for tig-mig hybrid welding process. *Journal of Manufacturing Processes* **2014**, *16*, 485-493.
12. Hsu, Y.F.; Rubinsky, B. Two-dimensional heat transfer study on the keyhole plasma arc welding process. *International Journal of Heat & Mass Transfer* **1988**, *31*, 1409-1421.
13. Wu, C.S.; Wang, L.; Ren, W.J.; Zhang, X.Y. Plasma arc welding: Process, sensing, control and modeling. *Journal of Manufacturing Processes* **2014**, *16*, 74–85.
14. Tashiro, S.; Miyata, M.; Tanaka, M.; Shin, K.; Takahashi, K. Numerical analysis of basic property of keyhole welding with plasma arc. *Trans.mat.res.soc.japan* **2010**, *35*, 589-592.
15. Stenbacka, N. On arc efficiency in gas tungsten arc welding. *Soldag. insp.* **2013**, *18*, 380-390.
16. Fuerschbach, P.W.; Knorovsky, G.A. A study of melting efficiency in plasma arc and gas tungsten arc welding. *Welding Journal* **1991**, *70*, S287-S297.
17. Sun, J.S.; Wu, C.S.; Zhang, Y.M. Heat transfer modeling of double-side arc welding. *Acta Physica Sinica* **2002**, *51*, 286-290.
18. Zhang, Y. Keyhole double-sided arc welding process. *Journal of Materials Science & Technology* **2001**, *17*, 159-160.
19. Wang, J.; Sun, Q.; Feng, J.; Wang, S.; Zhao, H. Characteristics of welding and arc pressure in tig narrow gap welding using novel magnetic arc oscillation. *The International Journal of Advanced Manufacturing Technology* **2017**, *90*, 413-420.
20. Cheng, L.; Hu, S.; Wang, Z. Arc pressure analysis in variable polarity tig welding. *Hanjie Xuebao/transactions of the China Welding Institution* **2014**, *35*, 101-104.
21. Huang, Y.; Huaiyu, Q.U.; Fan, D.; Liu, R.; Kang, Z.; Wang, X. Arc pressure measurement and analysis of coupling arc aa-tig. *Transactions of the China Welding Institution* **2013**.
22. Ham, H.S.; Oh, D.S.; Cho, S.M. Measurement of arc pressure and shield gas pressure effect on surface of molten pool in tig welding. *Science and Technology of Welding and Joining* **2013**, *17*, 594-600.
23. Ham, H.S.; Oh, D.S.; Cho, S.M. Measurement of arc pressure and shield gas pressure effect on surface of molten pool in tig welding. *Science & Technology of Welding & Joining* **2012**, *17*, 594-600.
24. Qi, B.J.; Yang, M.X.; Cong, B.Q.; Liu, F.J. The effect of arc behavior on weld geometry by high-frequency pulse gtaw process with 0cr18ni9ti stainless steel. *The International Journal of Advanced Manufacturing Technology* **2013**, *66*, 1545-1553.
25. Dashan, D.; Yonglun, S.; Leping, Z.; Yifeng, Z.; Hui, Z. Study on the pressure in plasma arc. *Chin J Mech Eng-En* **2003**, 34-36.

26. Murphy, A.B.; Tanaka, M.; Yamamoto, K.; Tashiro, S.; Sato, T.; Lowke, J.J. Modelling of thermal plasmas for arc welding: The role of the shielding gas properties and of metal vapour. *Journal of Physics D-Applied Physics* **2009**, *42*.
27. Murphy, A.B. Thermal plasmas in gas mixtures. *Journal of Physics D-Applied Physics* **2001**, *34*, R151-R173.